Supporting Information

Copper delocalization leads to ultralow thermal conductivity in chalcohalide $CuBiSeCl_2$

Yuzhou Hao,[1] Junwei Che,[2] Xiaoying Wang,[1] Xuejie Li,[1] Turab Lookman,[3] Jun Sun,[1] Xiangdong Ding,[1] and Zhibin Gao [1,*]

[1]*State Key Laboratory for Mechanical Behavior of Materials, School of Materials Science and Engineering, Xi'an Jiaotong University, Xi'an 710049, China*
[2]*Department of Applied Physics, Xi'an University of Science and Technology, Xi'an, 710054, China*
[3]*AiMaterials Research LLC, Santa Fe, New Mexico 87501, USA*

∗ E-mail: zhibin.gao@xjtu.edu.cn

Despite significant advancements in DFT-based thermal conductivity calculations [1], the computational cost of including higher-order phonon scattering remains prohibitive in many cases [2-6]. Machine Learning Potentials (MLPs) offer a promising solution by significantly lowering the computational burden associated with interatomic force constant calculations while preserving a high level of accuracy [7]. MLPs utilize machine learning algorithms to model the atomic potential energy surface, predicting both energy and forces based on the atomic environment. MLPs can be combined with BTE methods to provide detailed insights into phonon transport mechanisms in complex systems. Previous work has developed the neuroevolution potentials (NEP), a machine learning potential that strikes an effective balance between computational accuracy and efficiency [8, 9]. NEP can produce highly accurate second- and third-order force constants, and previous studies have demonstrated its ability to reliably compute fourth-order force constants, which are critical for accurately predicting κ_L in systems where four-phonon scattering plays a significant role [10].

In this case, the resulting root-mean-square error (RMSE) is presented in Fig. S1. The RMSE of energy per atom and atomic force is 0.00132 eV/atom and 0.07083 eV/ Å, respectively. These values indicate that the trained NEP is sufficiently accurate for calculating thermodynamic properties [8]. Furthermore, as shown in Fig. S2, the phonon spectrum calculated by NEP is in good agreement with the DFT results.

Building on this, we have adapted and enhanced the NEP interface to efficiently calculate the fourth-order force constants, enabling more accurate modeling of thermal transport in materials with strong anharmonic effects. For higher-order lattice anharmonicity, the homogeneous nonequilibrium molecular dynamics (HNEMD)

method with GPUMD package could be used to include full-order lattice anharmonicity [11-13].

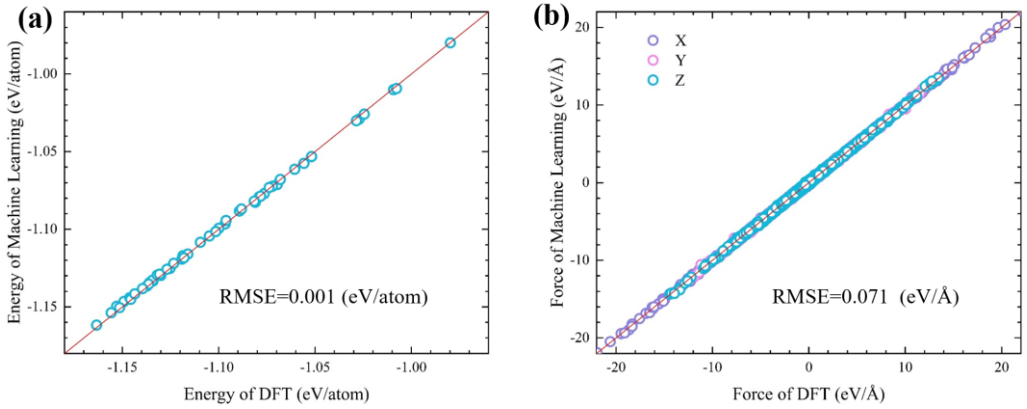

FIG. S1. The (a) energy per atom and (b) atomic force between neuroevolution potentials (NEP) and DFT calculations for $CuBiSeCl_2$.

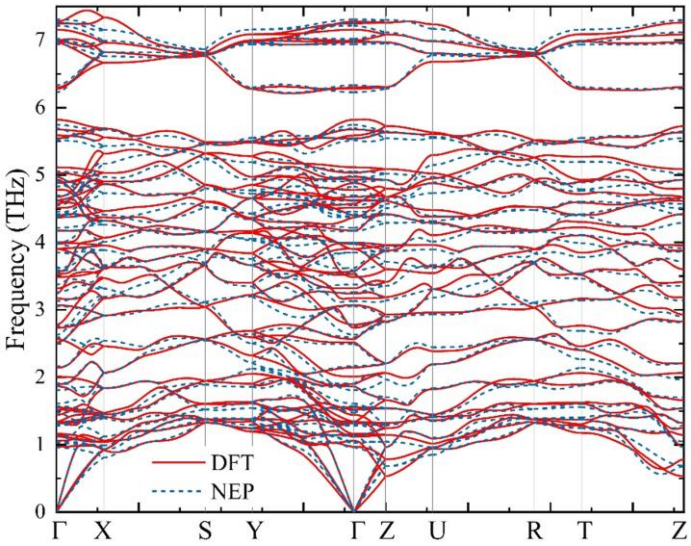

FIG. S2. Phonon dispersion of $CuBiSeCl_2$ calculated by neuroevolution potentials (NEP) and DFT along the high-symmetry path Γ-X-S-Y-Γ-Z-U-R-T-Z in the Brillouin zone.

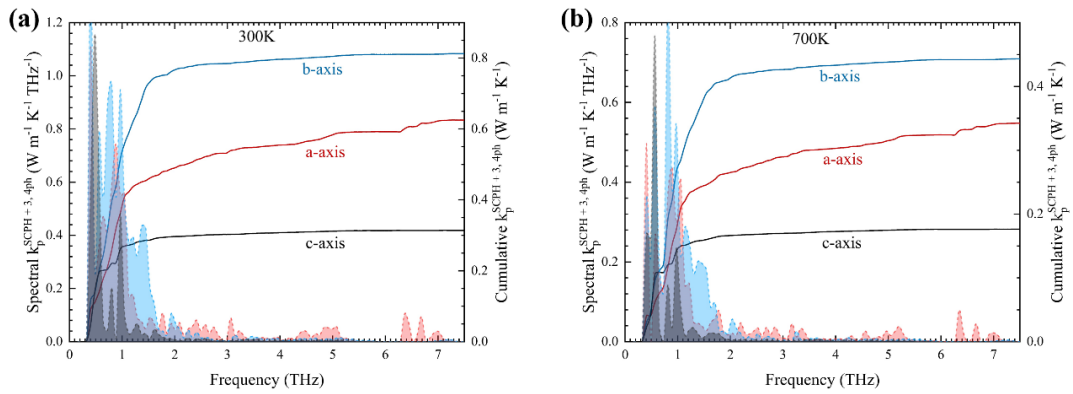

FIG. S3. Calculated spectral and cumulative κ_p of $CuBiSeCl_2$ at full frequency range using the SCPH+3,4ph model at (a) 300 K, (b) 700 K.

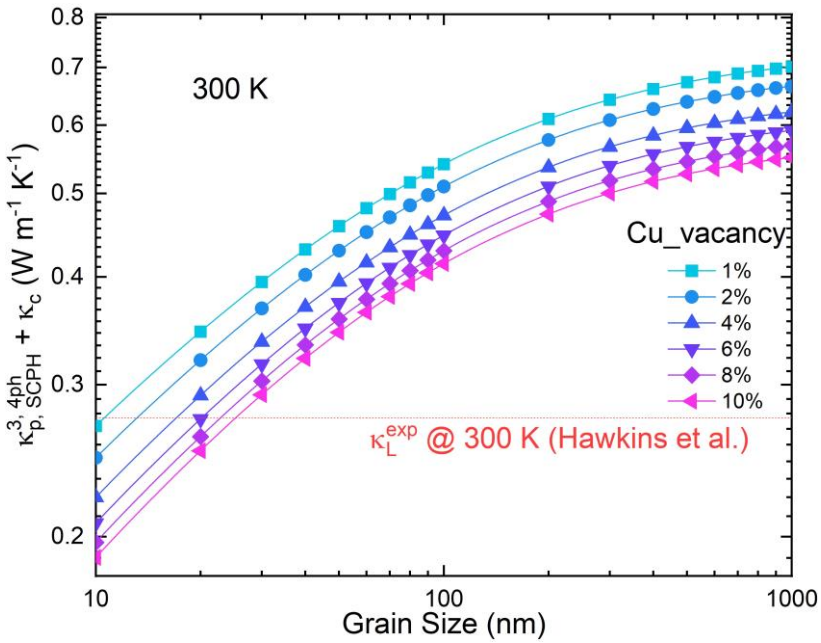

FIG. S4. Lattice thermal conductivity at 300 K considering both grain size and Cu vacancy defects compare with Hawkins experiment result.

Vacancies typically lead to a substantial reduction in the lattice thermal conductivity (κ_L) by introducing additional phonon scattering mechanisms. The scattering rate ($\tau_{\text{vacancy}}^{-1}$) caused by vacancies, denoted as:

$$\tau_{\text{vacancy}}^{-1} = \frac{9\pi}{2} f_v \omega^2 \text{pDOS}(\omega),$$

where f_v is the vacancy concentration, ω is the phonon frequency, and $\text{pDOS}(\omega)$ is the partial density of states of the atom species associated with the vacancy. The coefficient 9 accounts for mass and bond disorder effects. As a result, the residual discrepancies arise from unaccounted point defects (e.g., Copper vacancies) [14], as the shown in Figure S4.

Also scattering rates due to grain boundary ($\tau_{\text{gb},\lambda}^{-1}$) are calculated using the formulations shown in the following equation:

$$\tau_{\text{gb},\lambda}^{-1} = \frac{v_{\text{ph},\lambda}}{D_{\text{grain}}}.$$

Here, λ represents the phonon mode $(\mathbf{q}, j)$ with $\mathbf{q}$ and j labeling the phonon wave vector and dispersion branch, respectively. v_{ph} represents the phonon group velocity at λ, and D_{grain} is the grain size [14].

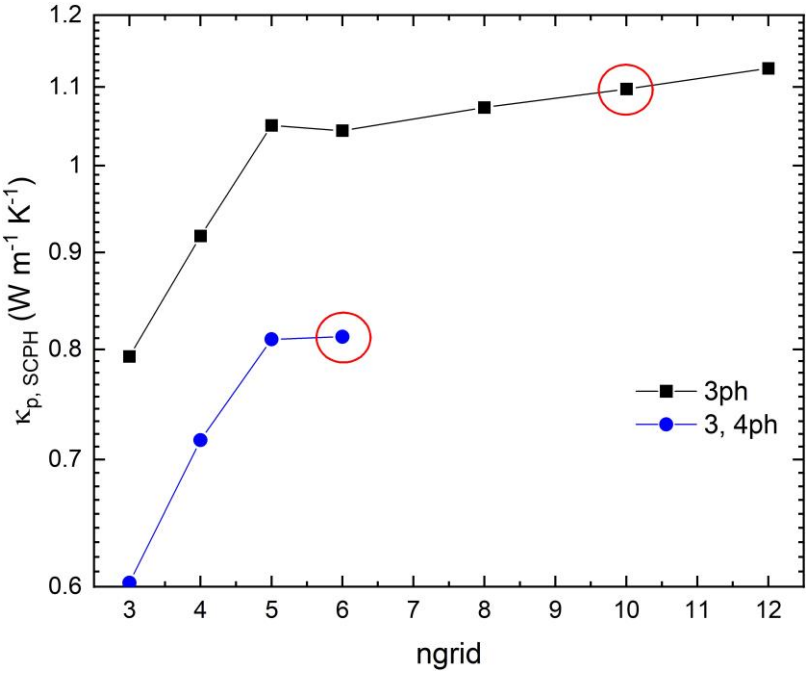

FIG. S5. Ngrid convergence test results for both 3ph and 3, 4ph calculation at 300 K.

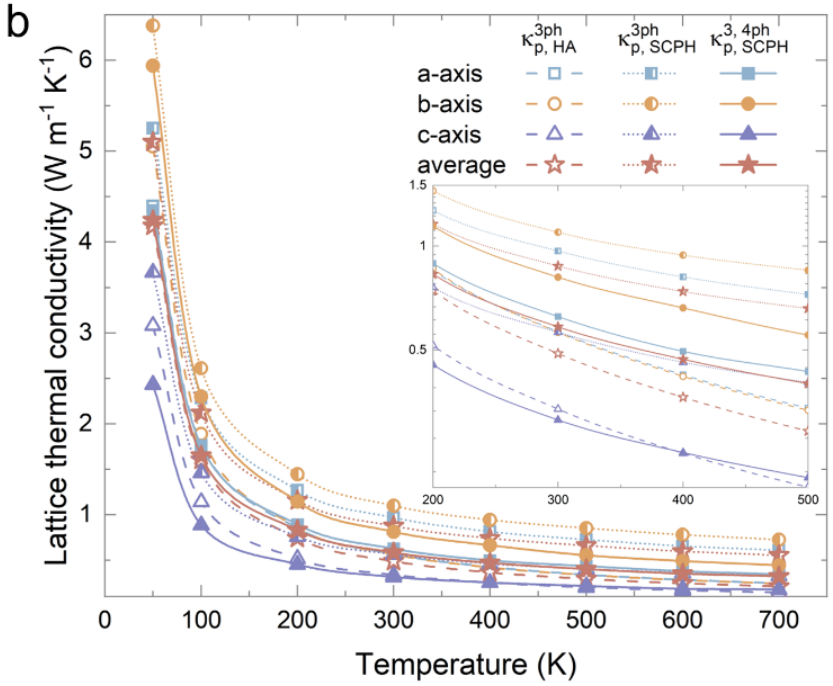

FIG. S6. κ_p of $CuBiSeCl_2$ using HA+3ph, SCPH+3ph, SCPH+3,4ph approaches with linear scale.

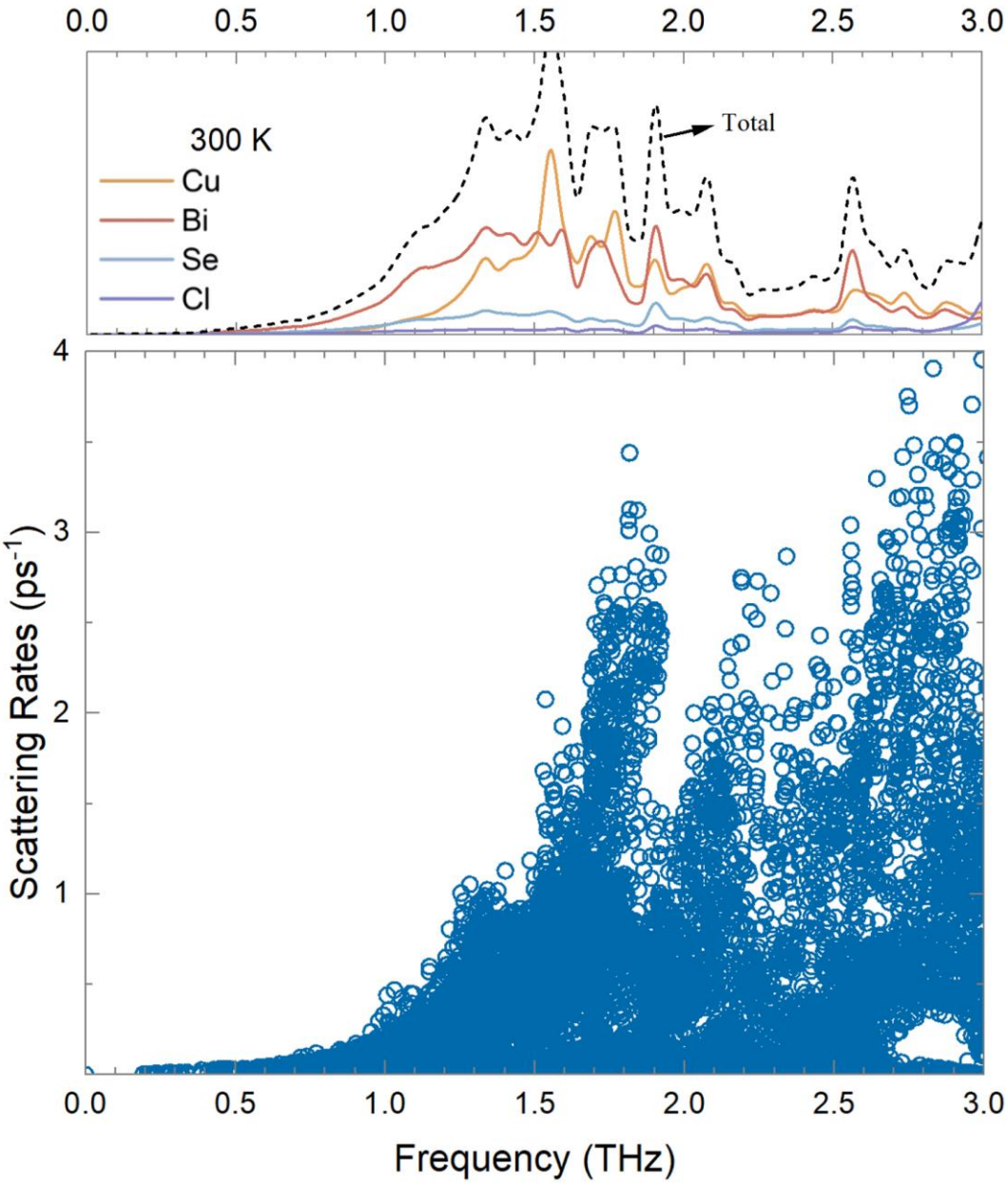

FIG. S7. Projected phonon density of states (PDOS) of $CuBiSeCl_2$ compared with the phonon scattering rates.

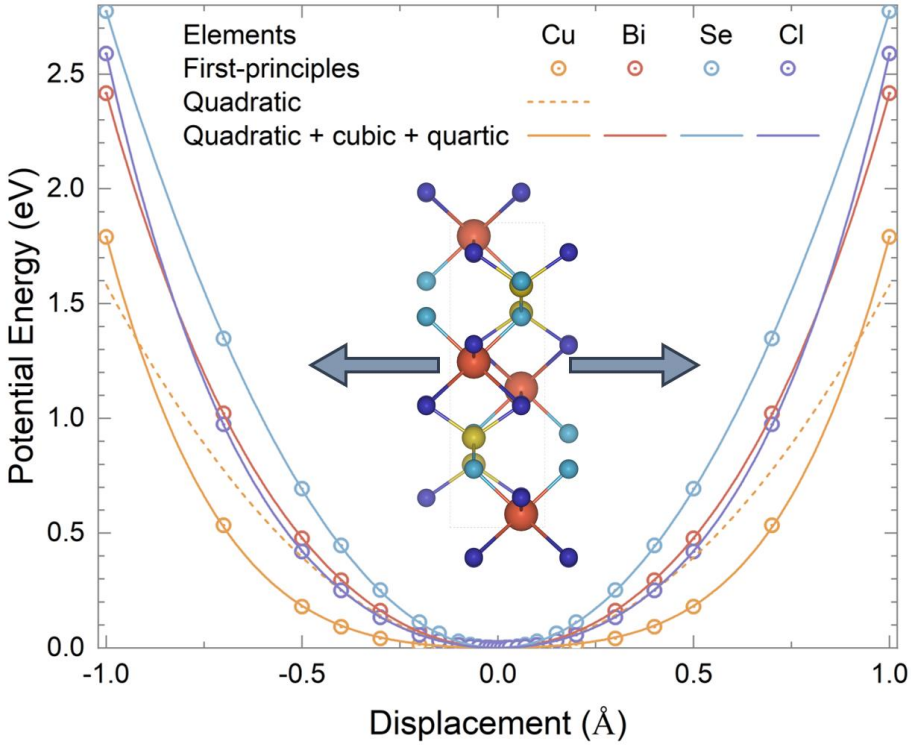

FIG. S8. Potential energy per atom with displacement of Cu (yellow) atoms along the *b*-axis direction with quartic and quadratic polynomial fitting. It writes as $y = 1.41x^4 - 3.19 \times 10^{-11}x^3 + 0.38x^2$ and $y = 1.58x^2$. For the Bi (red), Se (blue), and Cl (purple) atoms, the quartic polynomial fittings along the b-axis direction are as follows: $y = 0.67x^4 + 4.18 \times 10^{-10}x^3 + 1.75x^2$, $y = 1.20x^4 + 6.37 \times 10^{-11}x^3 + 1.39x^2$ and $y = 0.015x^4 + 1.94 \times 10^{-10}x^3 + 2.76x^2$. The cubic term is minimal and less than 10^{-5}.

Crystal structure

1.0

8.7276805046168864	0.0000000000000000	0.0000000000000000
0.0000000000000000	4.0527501406947950	0.0000000000000000
0.0000000000000000	0.0000000000000000	12.9853727996873882

Bi	Se	Cu	Cl
4	4	4	8

Direct

0.2684401075434918	0.2500000000000000	0.9561080459861631
0.7315598624565456	0.7500000000000000	0.0438919540137810
0.2315598924565005	0.7500000000000000	0.4561080459862369
0.7684401375434544	0.2500000000000000	0.5438919540138369
0.2392869357550447	0.7500000000000000	0.8082991440338070
0.7607130792449792	0.2500000000000000	0.1917008559661681
0.2607130792449543	0.2500000000000000	0.3082991440338082
0.7392869207550208	0.7500000000000000	0.6917008559661930
0.4625468533466238	0.7500000000000000	0.7054284410401965
0.5374531166534080	0.2500000000000000	0.2945715589598311
0.0374531466533878	0.2500000000000000	0.2054284410401549
0.9625468833465920	0.7500000000000000	0.7945715589598035
0.4356888236641090	0.2500000000000000	0.5970314360328625
0.5643111763359286	0.7500000000000000	0.4029685639671910
0.0643111763358971	0.7500000000000000	0.0970314360327938
0.9356888236640714	0.2500000000000000	0.9029685639671375
0.5617684115770415	0.2500000000000000	0.8985968561099364
0.4382315884229493	0.7500000000000000	0.1014031438900374
0.9382315884229585	0.7500000000000000	0.3985968561099719
0.0617684115770438	0.2500000000000000	0.6014031438900636

References:

[1] Li, W.; Carrete, J.; A. Katcho, N.; Mingo, N. ShengBTE: A solver of the Boltzmann transport equation for phonons. Comput. Phys. Commun. 2014, 185, 1747-1758.

[2] Han, Z.; Yang, X.; Li, W.; Feng, T.; Ruan, X. FourPhonon: An extension module to ShengBTE for computing fourphonon scattering rates and thermal conductivity. Comput. Phys. Commun. 2022, 270, 108179.

[3] Tong, Z.; Pecchia, A.; Yam, C.; Dumitrica, T.; Frauenheim, T. Glass-like Transport Dominates Ultralow Lattice Thermal Conductivity in Modular Crystalline $Bi_4O_4SeCl_2$. Nano Lett. 2023, 23, 9468-9473.

[4] Wang, Y.; Gao, Z.; Wang, X.; Sun, J.; Feng, M.; Hao, Y.; Li, X.; Zhao, Y.; Ding, X. Anomalous thermal conductivity in 2D silica nanocages of immobilizing noble gas atom. Appl. Phys. Lett. 2024, 124, 122205.

[5] Wang, X.; Feng, M.; Xia, Y.; Sun, J.; Ding, X.; Li, B.; Gao, Z. Revisiting lattice thermal conductivity of CsCl: The crucial role of quartic anharmonicity. Appl. Phys. Lett. 2024, 124, 172201.

[6] Feng, M.; Wang, X.; Zhu, G.; He, C.; Sun, J.; Ding, X.; Shiomi, J.; Xia, Y.; Li, B.; Gao, Z. The relation between the atomic mass ratio and quartic anharmonicity in alkali metal hydrides. Mater. Today Phys. 2024, 44, 101423.

[7] Mortazavi, B.; Podryabinkin, E. V.; Novikov, I. S.; Rabczuk, T.; Zhuang, X.; Shapeev, A. V. Accelerating first principles estimation of thermal conductivity by machine-learning interatomic potentials: A MTP/ShengBTE solution. Comput. Phys. Commun. 2021, 258, 107583.

[8] Fan, Z. et al. GPUMD: A package for constructing accurate machine-learned potentials and performing highly efficient atomistic simulations. J. Chem. Phys. 2022, 157, 114801.

[9] Dong, H.; Shi, Y.; Ying, P.; Xu, K.; Liang, T.; Wang, Y.; Zeng, Z.; Wu, X.; Zhou, W.; Xiong, S.; Chen, S.; Fan, Z. Molecular dynamics simulations of heat transport using machine-learned potentials: A mini-review and tutorial on GPUMD with neuroevolution potentials. J. Appl. Phys. 2024, 135, 161101.

[10] Ouyang, Y.; Yu, C.; He, J.; Jiang, P.; Ren, W.; Chen, J. Accurate description of high-order phonon anharmonicity and lattice thermal conductivity from molecular dynamics simulations with machine learning potential. Phys. Rev. B 2022, 105, 115202.

[11] Fan, Z.; Dong, H.; Harju, A.; AlaNissila, T. Homogeneous nonequilibrium molecular dynamics method for heat transport and spectral decomposition with many-body potentials. Phys. Rev. B 2019, 99, 064308.

[12] Evans, D. J. Homogeneous NEMD algorithm for thermal conductivityApplication of non-canonical linear response theory. Phys. Lett. A 1982, 91, 457-460.

[13] Gabourie, A. J.; Fan, Z.; Ala-Nissila, T.; Pop, E. Spectral decomposition of thermal conductivity: Comparing velocity decomposition methods in homogeneous molecular dynamics simulations. Phys. Rev. B 2021, 103, 205421.

[14] Tiwari, Janak; Feng, Tianli Intrinsic thermal conductivity of ZrC from low to ultrahigh temperatures: A critical revisit. Phys. Rev. Mater. 2023, 7, 6.